Measurement 194 (2022) 111061

Contents lists available at ScienceDirect

Measurement

journal homepage: www.elsevier.com/locate/measurement

Effect of the number of projections in X-ray CT imaging on image quality and digital volume correlation measurement

Zhang Xuanhao [a], Sun Lijuan [b], Wang Bo [a], Pan Bing [a,*]

[a] Institute of Solid Mechanics, Beihang University, Beijing 100191, China
[b] Institute of Mechanics, Chinese Academy of Sciences, Beijing, 100190, China

ARTICLE INFO

Keywords:
Digital volume correlation
Number of projections
X-ray computed tomography
FDK algorithm

ABSTRACT

Digital volume correlation (DVC) quantifies internal 3D displacement and strain fields by correlating the volume images of a tested object acquired at different states. When using X-ray CT-based DVC, the number of projections is a key parameter that affects the acquisition time and quality of reconstructed volumetric images, and therefore the precision and temporal resolutions of DVC measurement. More projections result in high-quality volume images for DVC calculation but longer acquisition time and pronounced thermal drifts of the X-ray source. Few projections lead to quicker acquisition and fewer thermal drifts, but may degrade image quality and thus induce larger DVC measurement errors. Selecting an appropriate number of projections during CT imaging is therefore of practical significance for DVC measurement. To solve this dilemma, the effect of the number of projections on DVC measurements with X-ray CT is experimentally investigated in this work. First, numerically simulated speckle volume images with different numbers of projections were reconstructed by using FDK (Feldkamp) algorithm, and the influence of the number of projections on DVC measurement was analyzed. Then, real rescan and compression experiments performed on a copper foam sample were carried out to further study the effect of projection number on DVC measurements. Both simulation and real experiments show that more projections result in longer imaging time but higher quality volume image and DVC measurement. DVC measurement errors decrease with the increase of projections at different decline rates. Therefore, an appropriate number of projections can be specified based on the results according to the requirements of DVC measurement precision and temporal resolution. For the specific X-ray CT device used in this real compression experiment, 36 ~ 60 projections are suggested to balance measurement precision and temporal resolution, and more than 720 projections are necessary for pursuing higher accuracy.

1. Introduction

Originally extended from two-dimensional digital image correlation by Bay BK et al. in 1999[1], digital volume correlation (DVC) has evolved into a practical and powerful experimental technique for interior full-field 3D displacement and strain measurement. As an image-based deformation measuring technique, DVC deals with volume images of a test object acquired by a volumetric imaging device at different loading states. Volumetric images are typically acquired from X-ray Computed Tomography (X-ray CT) systems for opaque solid materials [2–4], Magnetic Resonance Imaging (MRI) [5] or Optical Coherence Tomography (OCT) systems for biological subjects[6,7], or Laser Scanning Confocal Microscopes (LSCM) for transparent media[8]. Among these volume imaging devices, laboratory or industrial X-ray CT devices are undoubtedly the most widely used in DVC measurements due to their easy access and simple operation.

The imaging principle of an X-ray CT machine is schematically shown in Fig. 1. CT imaging consists of two steps: projection images collection and volume image reconstruction. In the first step, the tested sample mounted on a rotary stage is exposed to an X-ray source and rotates by step. The two-dimensional projection (i.e., an attenuated X-ray image) of the tested sample at each rotation step is recorded by the detector. Then, the volume image of the tested sample can be reconstructed via a certain reconstruction algorithm (e.g., the Feldkamp algorithm[9]).

In the process of projection collection, many parameters specified by the operator would affect the acquisition time and quality of the reconstructed volume images[10,11]. These parameters include, but are

* Corresponding author.
E-mail address: panb@buaa.edu.cn (P. Bing).

https://doi.org/10.1016/j.measurement.2022.111061
Received 30 November 2021; Received in revised form 14 February 2022; Accepted 19 March 2022
Available online 23 March 2022

not limited to, X-ray source power, voltage, exposure time, the number of projections (N_{proj}) [12]. Among these parameters, the number of projections is the important factor in volume image quality and imaging time [13,14], which further have a significant impact on the precision and temporal resolution of DVC measurement. In other words, X-ray CT-based DVC measurement faces a dilemma in selecting an appropriate N_{proj} for optimal spatiotemporal resolution. On one hand, the accuracy of DVC relies heavily on the quality and fidelity of the reconstructed volume images (intensity gradient, noise level, etc)[15,16]. According to the spatial Nyquist sampling theorem in the field of CT imaging[17], larger N_{proj} can provide complete data to reconstruct the volume images with better image quality and few image artifacts[18], which is conducive to enhancing the quality of DVC measurements[19]. On the other hand, the imaging time is highly associated with the temporal resolution of DVC measurement. Larger N_{proj} leads to longer data acquisition time, which might be undesirable in DVC-based *in-situ* mechanical testing because of less temporal resolution. Besides, too long data acquisition time may cause some unnecessary imaging errors, such as the imaging distortion induced by the thermal drifts of the X-ray source[3,20].

Recently, the effect of the number of projections on reconstruction quality and DVC displacement error was investigated briefly in Ref.[15]. However, this research pays little attention to providing constructive suggestions on solving this dilemma in selecting N_{proj} for optimal DVC measurement. Up to now, how to choose an appropriate N_{proj} to balance temporal resolution and measurement quality during practical DVC applications remains an important but confusing problem facing DVC practitioners. To address this dilemma, it is of great practical significance to study the two-sided influence of the number of projections on DVC measurement, and more importantly, provide suggestions for selecting an appropriate number of projections in real DVC applications.

This work aims to experimentally study the effect of the number of projections in X-ray CT imaging on image quality and DVC measurement, and provide certain referential suggestions for the appropriate selection of this key parameter. In the remainder of this paper, the Feldkamp (FDK) algorithm used for volume image reconstruction and the DVC algorithm employed for internal 3D displacement extraction are first briefly introduced. Then, simulated X-ray CT imaging experiment and real rescan and compression experiments of a copper foam sample were carried out to experimentally investigate the effect of the number of projections on DVC measurement. The experimental procedures and DVC measurement analysis are detailed presented. Some valuable conclusions and corresponding suggestions to select an appropriate number of projections are also discussed.

2. Methods

In this section, the FDK algorithm, the classic volume image reconstruction algorithm, which was used to reconstruct volume images with different numbers of projections collected in X-ray CT imaging, is described first. Then the basic principle of subvolume-based local DVC method, which was employed for extracting sub-voxel displacement from volume images, is introduced.

2.1. FDK algorithm for reconstruction

At present, the mainstream commercial CT machine in the industrial field is the cone-beam computed tomography (CBCT) scanner, which possesses a higher ray utilization rate and faster acquisition than the traditional two-dimensional fan-beam CT. The volume images can be reconstructed from the collected cone-beam projection data by different CBCT reconstruction algorithms. Among these algorithms, the FDK algorithm is commonly used for reconstruction with angularly equidistributed projections in CBCT systems owing to its advantages of circle track scanning, simple structure, and excellent reconstruction efficiency. The method of limited-angle tomographic reconstruction also has been further developed in recent years[21]. Since the angularly equidistributed projections are provided in this work, the FDK algorithm is used to study the effect of the number of projections in X-ray CT imaging on DVC measurement.

To facilitate understanding the FDK algorithm, the geometric structure of CBCT scanner is shown in Fig. 2, where *Oxyz* is the fixed coordinate system of reconstructed volume image and *Ouvw* is the rotating coordinate system. *v*-axis coincides with *z*-axis and the source on *w*-axis rotates around the central *z*-axis. *R* and β denote the radius and angle of the rotation, respectively. *Ouv* is the virtual detector plane, which is parallel to the detector and contains the rotation axis. Supposing that the position of the point *P* on the virtual detector plane corresponding to the

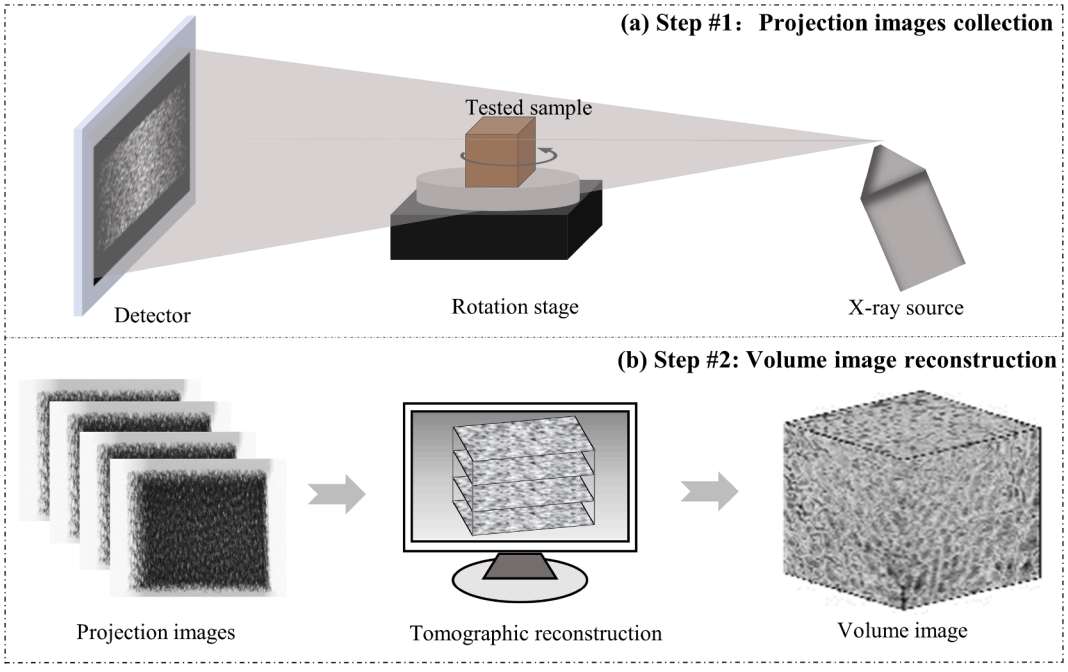

Fig. 1. X-ray CT imaging step: (a) projection images collection and (b) volume image reconstruction.

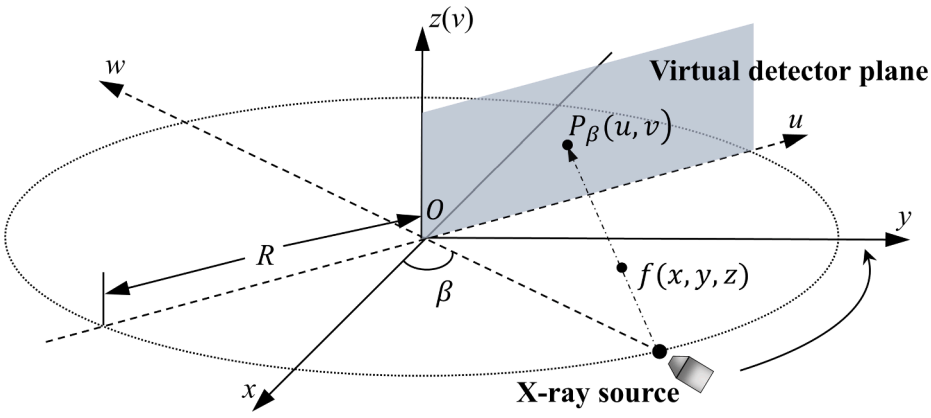

Fig. 2. Geometric structure of FDK.

voxel point $f(x,y,z)$ in reconstructed volume image is (u,v), the projection value of P is denote by $P_\beta(u,v)$ (See Fig. 2). P is the point on the virtual detector in Fig. 2 and p in Fig. 3 is the calculation point.

The implementation of the FDK algorithm mostly consists of three steps: 1) weighted correction processing, 2) horizontal filtering processing, and 3) weighted back-projection processing[9] as described step by step as follows:

Step #1: Weighted correction processing. The two-dimensional projection data $P_\beta(u,v)$ is corrected by weighting factor:

$$P'_\beta(u,v) = \frac{R}{\sqrt{R^2+u^2+v^2}} \cdot P_\beta(u,v) \tag{1}$$

where $P'_\beta(u,v)$ denotes the projection after the correction of the weighting factor.

Step #2: Horizontal filtering processing. The weighted data are horizontal filtered line by line:

$$P''_\beta(u,v) = P'_\beta(u,v) * h(u) \tag{2}$$

where $*$ denotes convolution and $h(u)$ represents a filter function (i.e., Ram-Lak filtering function[22]) for convoluting the projection image data of the u row.

Step #3: Weighted back projection processing. The filtered projection data are used for back projection calculation:

$$f(x,y,z) = \int_0^{2\pi} U^2 \cdot P''_\beta(u,v) d\beta = \sum_\beta U^2 \cdot P''_\beta(u,v) \tag{3}$$

where $u = U(x\cos\beta + y\sin\beta), v = Uz, U = R/(R + y\cos\beta - x\sin\beta)$.

2.2. Digital volume correlation

DVC is an image-based experimental mechanics tool, which retrieves full-field displacement and strain by comparing two digital volume images of a test object acquired at different states with a volumetric imaging machine. The volume images obtained before and after external loading are called reference and deformed volume images, respectively. Basic principles and registration implementations of subvolume-based local DVC have been explained clearly in previously published papers [23,24]. For completeness, the DVC algorithm is briefly described hereafter. During the routine implementation of DVC, a volume of interest (VOI) should be first specified in the reference volume image, which is further divided into virtual grids according to the specified grid step. The resulting evenly spaced grid points are known as discrete calculation points or points of interest (POI). To accurately determine the 3D displacement vector of each POI, a reference cubic sub-volume with a proper side length centered at a calculation point $p(x, y, z)$ is selected. Note that the reference subvolumes should contain sufficient local intensity variations to warrant they can be uniquely registered in the deformed volume images. The reference subvolume is searched using a certain correlation algorithm in deformed volume images to find a target subvolume with maximum similarity, and the coordinate differences between the target subvolume center and the reference subvolume center yield the desired displacement vector of the POI. The same matching process is repeated at each POI to obtain the full-field 3D deformation.

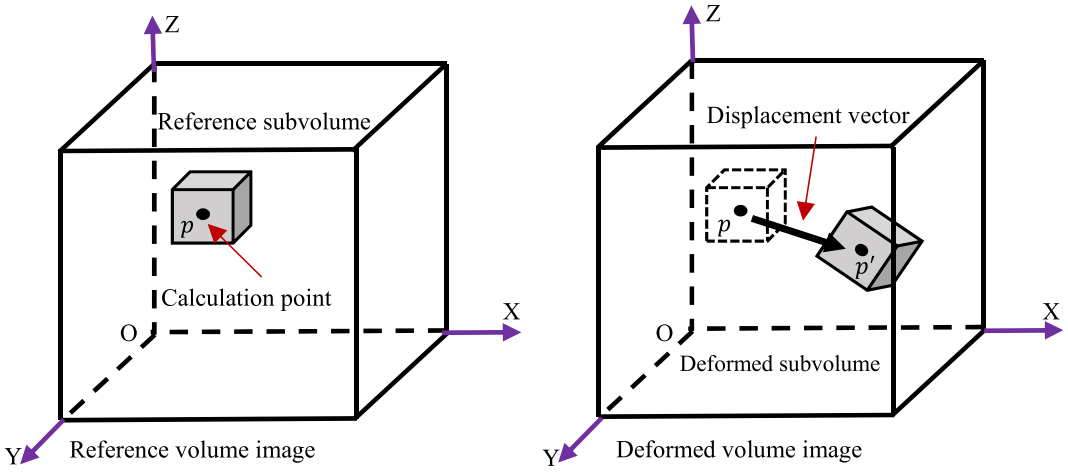

Fig. 3. Schematic illustration showing the basic principle of digital volume correlation.

To quantify the gray level similarity between the reference and target sub-volumes, a correlation criterion, together with a certain shape function that describes the shape and position change of sub-volumes, should be defined. The most commonly used correlation function is the zero-mean normalized sum-of-square difference (ZNSSD) function, which is equivalent to the well-known zero-mean normalized cross-correlation (ZNCC) criterion[25].

$$C_{ZNSSD}(p) = \sum_{\xi}\left\{\frac{[f(x)-f_m]}{\Delta f} - \frac{[g(x^{'})-g_m]}{\Delta g}\right\}^2 \tag{4}$$

where $f(\mathbf{x})$ and $g(\mathbf{x}^{'})$ are the gray intensity of the reference and target deformed sub-volumes, respectively. $\mathbf{x}$ and $\mathbf{x}^{'}$ are the image coordinates of voxel points in the reference and target deformed sub-volumes. $\xi = (\Delta x, \Delta y, \Delta z)^T$ denotes the local coordinates in the reference sub-volume. f_m and g_m are the mean gray values of the reference and target deformed subvolumes. $\Delta f = \sqrt{\sum_{\xi}(f(\boldsymbol{x})-f_m)^2}$ and $\Delta g = \sqrt{\sum_{\xi}(g(x^{'})-g_m)^2}$. The unknown displacement vector to be determined is $\boldsymbol{p} = \left(u, u_x, u_y, u_z, v, v_x, v_y, v_z, w, w_x, w_y, w_z\right)^{\mathrm{T}}$. Note that the first-order shape function is employed to achieve a balance between computational efficiency and accuracy. When using the first-order shape function, the corrdinate of voxle points in target subvolumes can be written as

$$x^{'}(p) = x + \begin{bmatrix} u \\ v \\ w \end{bmatrix} + \begin{bmatrix} u_x & u_y & u_z \\ v_x & v_y & v_z \\ w_x & w_y & w_z \end{bmatrix} \begin{bmatrix} \Delta x \\ \Delta y \\ \Delta z \end{bmatrix} \tag{5}$$

The deformation parameters of **p** can be obtained by optimizing the non-linear ZNSSD correlation function. Firstly, the integer-voxel displacement of a seed point should be estimated by employing an integer-voxel searching algorithm. Subsequently, a subvoxel registration algorithm (i.e., 3D inverse compositional Gauss-Newton[23]) combined with an initial estimate transfer strategy (i.e., Reliability-guided displacement tracking, RGDT[26]) is used to determine the sub-voxel displacement. Since the coordinates of voxel points in the target deformed sub-volume normally fall into the sub-voxel positions after each iteration, a sub-voxel intensity interpolation scheme (i.e., Cubic B-spline interpolation scheme) is necessary when optimizing the correlation function iteratively. By repeating the correlation analysis at all calculation points, full-field displacement can be extracted.

3. Experiments

In practical X-ray CT imaging, the sampling interval Δ is fixed and the full rotation is generally between 0 and 2π. Then, the number of recorded projections is $N_{\mathrm{proj}} = 2\pi/\Delta$ and different N_{proj} can be obtained by changing Δ. To avoid other unnecessary errors in the process of projection collection, different numbers of projections were acquired in simulation and real experiments by evenly extracting from the maximum number (1440) of projection images.

3.1. Simulation experiment

First, to better investigate the effect of projection number of an X-ray CT scanner on the quality of reconstructed volume images and DVC measurements without imaging errors (e.g., Beam Hardening artifact [11] and ring artifact[27]) caused by imperfect X-ray imaging, computer-simulated translation and compression experiments were carried out firstly. As shown in Fig. 4, the simulation experiment consists of the following three steps:

Step #1: Volume images simulation. A simulated speckle volume image with the size of 200 × 200 × 200 voxels was first generated according to the method described in Ref.[24]. Then the rigid body translation (1.4 voxels in X direction, 1.2 voxels in Y direction, and 1.6 voxels in Z direction) and the first-order deformation in Z direction ($w = 0.02z$) were, respectively, applied to the original reference volume image to generate two deformed volume image I (translation) and II (compression).

Step #2: Projections extraction. The original reference volume image and original deformed volume images I and II are all projected to generate 1440 projections with the size of 300 × 300 pixels (i.e., the scanning interval is 0.25°, sampling within 0 ~ 2π). And then different numbers of projections are evenly extracted from these 1440 projections. 4, 8, 16, 36, 60, 90, 120, 180, 240, 360, 720, and 1440 projections were analyzed in this work. Electronic Gauss noise with a mean value of 0 and standard deviation of 10 is imposed on these projections to simulate the noise in the real projection sampling.

Step #3: Volume images reconstruction. The FDK algorithm is used to reconstruct the reference volume images and deformed volume images for DVC calculation from these different numbers of projections. During DVC calculation, the grid step is set as 10 voxels and the number of calculation points is 15 × 15 × 15 = 3375.

3.2. Real experiment

Real rescan and compression experiments were carried out to verify the simulation experiment results. As shown in Fig. 5, a foam copper sample with a size of 20 *mm* × 20 *mm* × 10 *mm* was chosen in the real experiment for its better natural texture features and the high-density polyethylene (HDPE) indenter was used to load in this experiment to reduce the artifact caused by the metal indenter. The sample is imaged by the X-ray CT (YXLON CT Modular, Germany). The X-ray source excitation voltage is set to 155 kV and the current is 0.4 mA. The source-to-detector and source-to-object are 999.99 *mm* and 81.87 *mm*, respectively. Then 1440 projection images with 1024 × 1024 pixels were obtained with a scanning interval of 0.25° and an exposure time of 0.7 s. Micro X-ray CT device and foam copper sample are shown in Fig. 5. The size of the reconstructed volume image is 1024 × 1024 × 800 voxels and

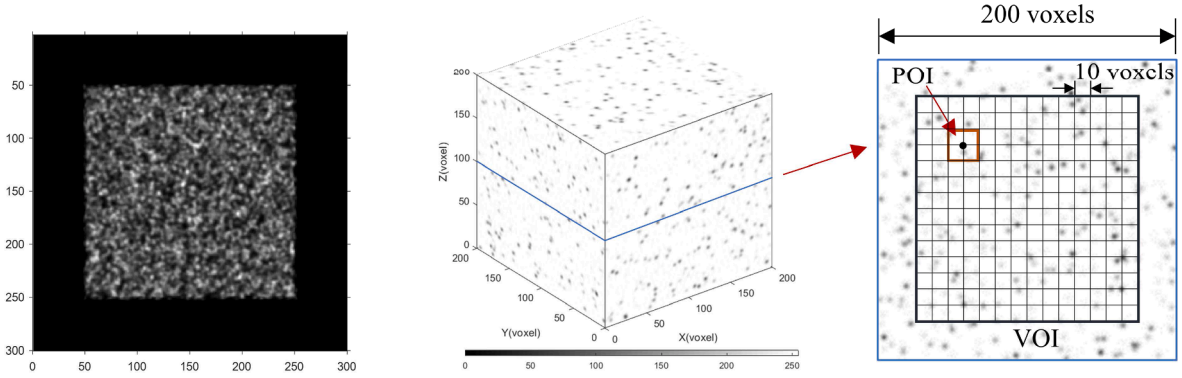

Fig. 4. Projection image (left), simulated volume image (middle) and sice image in simulation experiment (right).

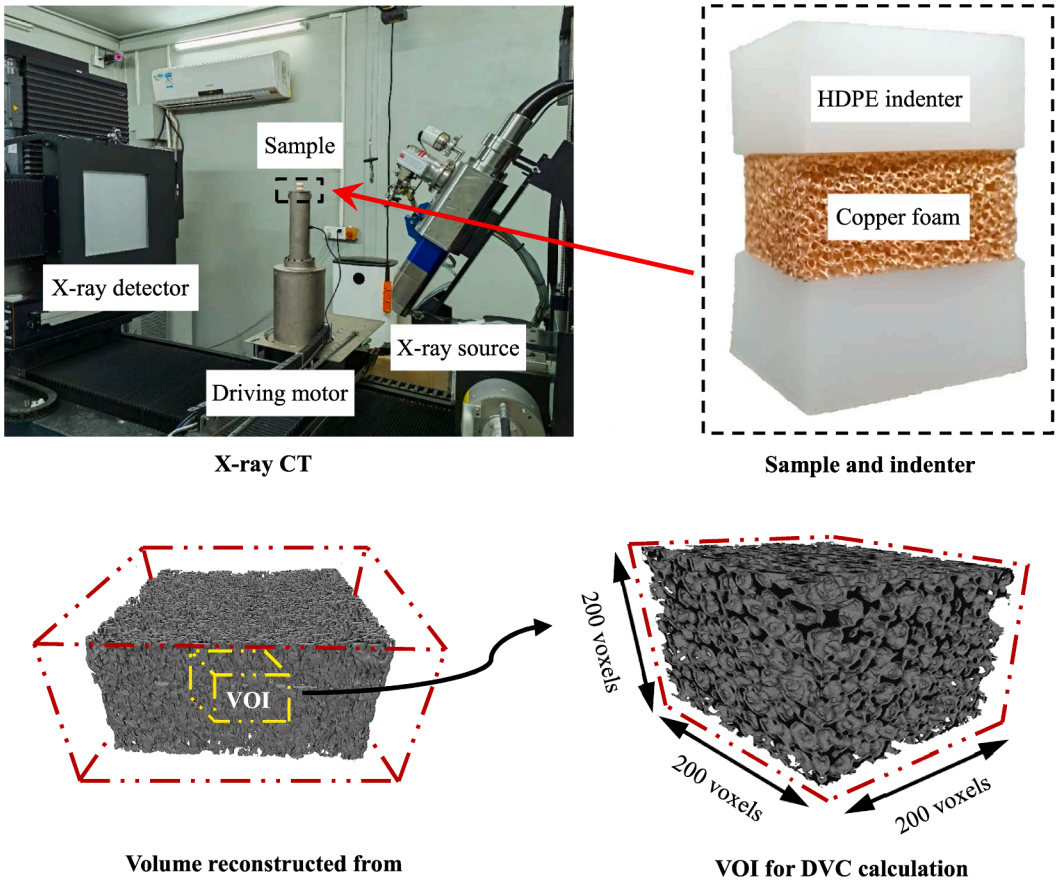

Fig. 5. Top: X-ray CT, copper foam sample, and Bottom: VOI of volume image for DVC calculation.

a 200 × 200 × 200 voxels VOI was selected for DVC calculation. The grid step was set to be 10 voxels and the number of calculation points is 15 × 15 × 15 = 3375, which are consistent with the simulation experiment.

The foam copper rescan experiment was carried out first. The foam copper sample was preloaded with a force of 20 N to ensure good end contact before testing. Then the sample was scanned twice in a static state and 1440 projections were acquired each time. Different numbers of projections were extracted evenly from 1440 projections to reconstruct the volume images by FDK algorithm and DVC calculation was carried out on these volume images. The foam copper compression experiment was carried out subsequently. The loading rate was set to 0.1 mm/min and the displacement loading distance was 0.1 mm. After loading, the sample was settled for 5 min to ensure enough stress relaxation time. Then scanning was performed to record the 1440 projections in the deformation state. The reconstruction and DVC calculation parameters are the same as the rescan experiment.

3.3. DVC analysis and error evaluation

The DVC method used in this work refers to Ref.[23], which utilizes the state-of-art 3D IC-GN algorithm combined with the cubic B-spline interpolation method for sub-voxel registration. The iterative convergence condition is set as follows: $\sqrt{(\Delta u)^2+(\Delta v)^2+(\Delta w)^2} \le 0.001\text{voxels}$ or the maximum number of iterations reaches 10. To investigate the influence of sub-volume size on DVC measurements with different numbers of projections, two different sub-volume sizes, 21 × 21 × 21 voxels and 41 × 41 × 41 voxels, were selected respectively in DVC calculation. The three-dimensional pointwise least-square (PLS) method with 11^3 calculation points is used to extract the positive strain field from the displacement field. All the DVC calculations were implemented using in-house DVC software written in C++ language on a desktop computer (Intel(R) Core(TM) i5-8250 CPU with a 1.60 GHz main frequency and 8 GB RAM).

The CT projection and reconstruction code used in this work is based on an open-source program TIGRE[28], which can obtain the projections under the CBCT system by projecting the volume images and reconstructing the volume images from different numbers of projections by FDK algorithm.

To better examine the effect of the number of projections on DVC measurement error, all DVC measurement results are analyzed in terms of relative error calculated based on DVC measurement with the maximum projection number since there are always some errors in DVC calculation itself.

$$u_e^i = \frac{\sum_{j=1}^{N}(u_j^i - u_j^m)}{N} \tag{6}$$

$$\sigma_u^i = \sqrt{\frac{\sum_{j=1}^{N}(u_j^i - u_j^m - u_e^i)^2}{N-1}} \tag{7}$$

where u_e^i, σ_u^i are mean error and standard deviation error of DVC measurements on volume images reconstructed from i projections. u_j^i represents the DVC-measured displacement or strain of j^{th} calculation point when using i projections to reconstruct. $m(m > i)$ is the maximum number of projections (m is 1440 in this work).

4. Results and discussion

4.1. Simulated translation and compression experiments

Fig. 6 shows the peak signal-to-noise ratio (PSNR) of reconstructed

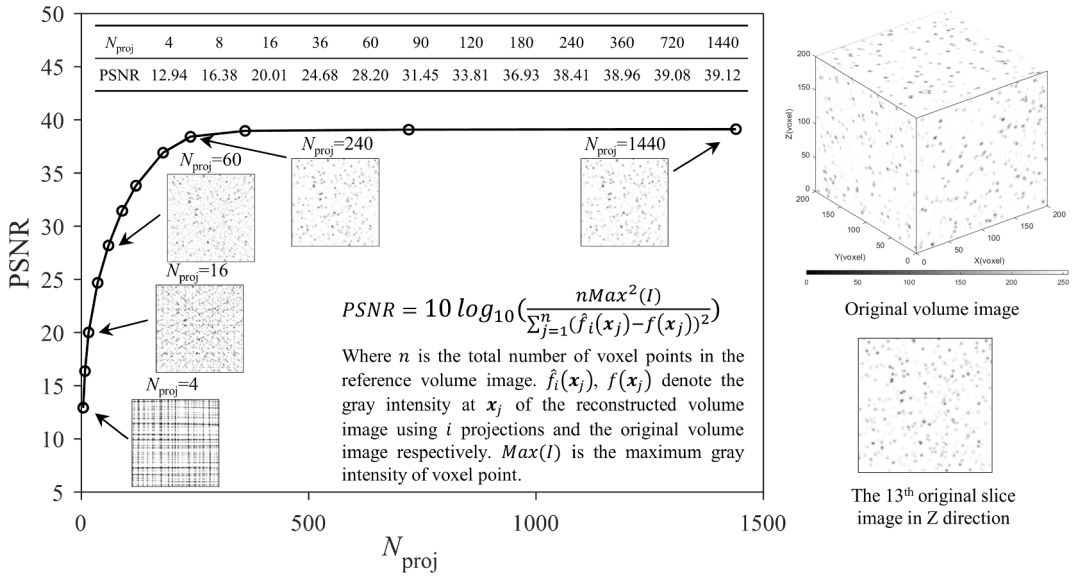

Fig. 6. The PSNR of reconstructed volume images with different N_{proj} in the simulation experiment, the original slice image, and the slice images reconstructed with N_{proj} = 4, 16, 60, 240 and 1440.

volume images with different N_{proj} in the simulation experiment. As shown in Fig. 6, with the increase of N_{proj}, the PSNR raises rapidly at first and then remains unchanged basically when N_{proj} exceeds 240. The slice images with 4 projections are significantly different from the original volume image and the slice image soon has more detailed information and less noise with the increase of N_{proj}. The slice image with N_{proj} = 240 is principally the same as the original slice image and further increasing N_{proj} improves the image quality little.

DVC calculation was carried out on these reference and deformed volume images reconstructed from different numbers of projections. Figs. 7 and 8 show the displacement and strain results of DVC measurements with two sub-volume sizes in the simulated translation experiment and the simulated compression experiment. As shown in Figs. 7 and 8, with the increase of the number of projections used in

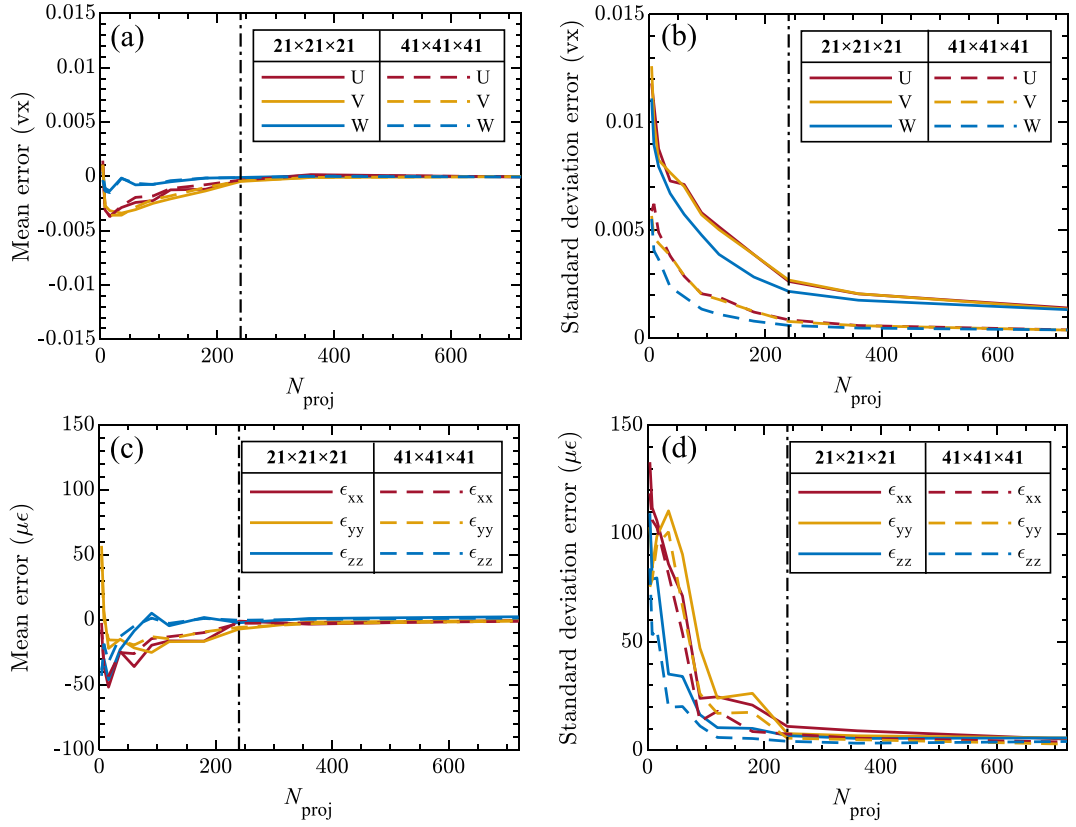

Fig. 7. Statistical results of DVC measurements on volume images reconstructed with different N_{proj} using two different sub-volume sizes in the simulated translation experiment: (a) mean error and (b) SD error in measured displacements, (c) mean error and (b) SD error in measured strains. Here the dash-dotted line is N_{proj} = 240, and vx denotes voxel.

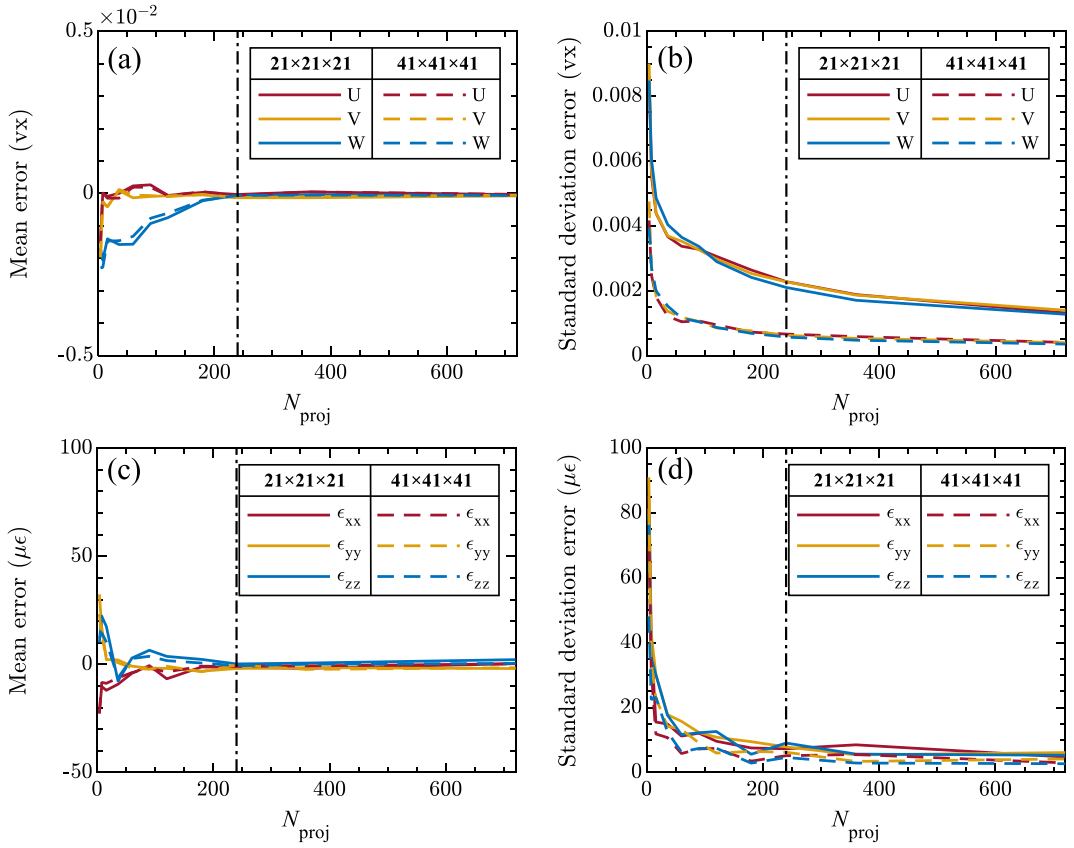

Fig. 8. Statistical results of DVC measurements on volume images reconstructed with different N_{proj} using two different sub-volume sizes in the simulated compression experiment: (a) mean error and (b) SD error in measured displacements, (c) mean error and (b) SD error in measured strains. Here the dash-dotted line is $N_{proj} = 240$, and vx denotes voxel.

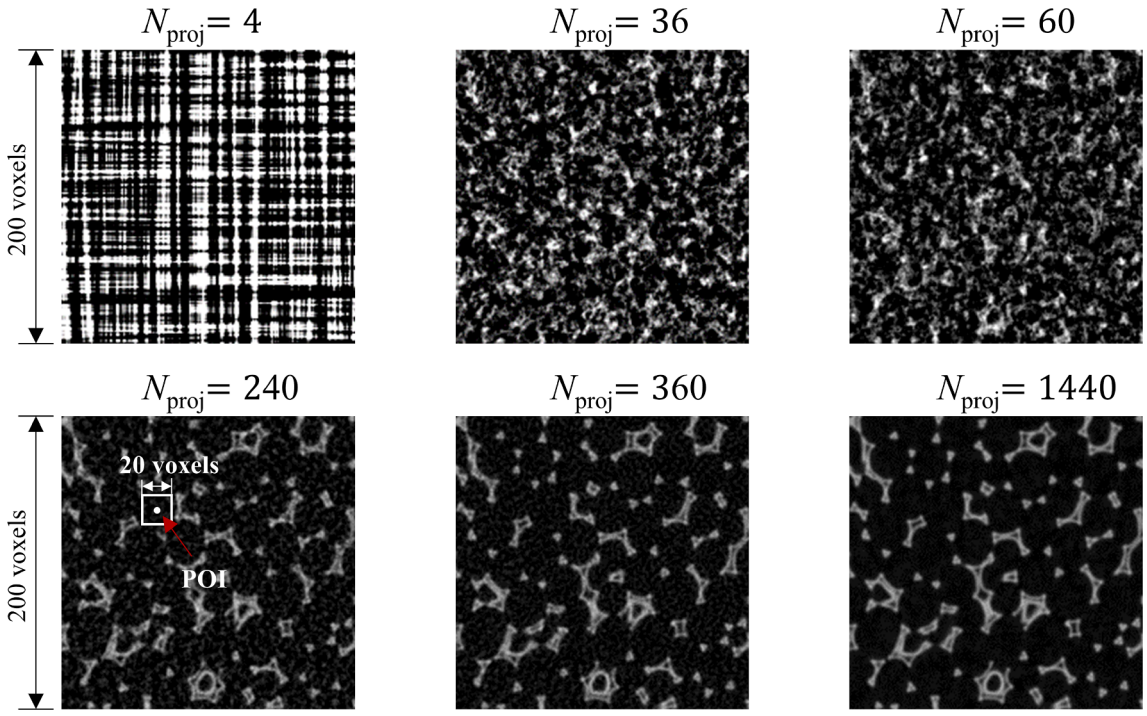

Fig. 9. The reconstructions with $N_{proj} = 4$, 36, 60, 240, 360 and 1440 in the real experiment. Each panel shows a slice image along the Z direction of the reconstructed volume image.

reconstructing volume images, the standard deviation error of displacement and strain gradually decreases, and the mean error of them remains unchanged after slight fluctuations. Increasing the sub-volume size helps to reduce the standard deviation error in displacement caused by volume images reconstructed with insufficient projections but have less effect on the standard deviation error of strain. Further analyzing of DVC measurements, it can be found that the decline rates of standard deviation error under different numbers of projections are not the same. The standard deviation errors in the simulated translation experiment, especially for the strain, decrease rapidly at the beginning while decreasing gently when N_{proj} slightly exceeds 240. Moreover, the mean errors no longer fluctuate and hold less level when N_{proj} exceeds 240. The errors in simulated compression experiments show similar trends.

4.2. Foam copper rescan and compression experiments

Fig. 9 shows slice images of volume images reconstructed with different numbers of projections in the real experiment. The PSNR is not calculated since there is no original volume image in the real experiment. The structure of copper foam can be hardly seen from the slice image with fewer than 60 projections. The slice image with 240 projections still has a small amount of noise but the interior structures can be roughly seen from this slice image. The slice image has little noise and the edge of the copper foam structure can be seen clearly when $N_{proj} = 1440$.

The DVC displacement measurements with 1440 projections in foam copper rescan and compression experiments are shown in Fig. 10. As shown in Fig. 10, the U, V, W displacement field can be extracted accurately by DVC measurement with 1440 projections.

As shown in Figs. 11 and 12, the standard deviation errors of DVC displacement and strain measurements also show a downward trend with the increase of N_{proj} and increasing the sub-volume size can reduce the standard deviation error caused by reconstructing volume images with insufficient projections, which are accordant with the simulation experiment results. The mean error of W direction displacement in the compression experiment has some differences from that in the rescan experiment. From Fig. 12 (a), we can see that the mean error increases greatly when N_{proj} is less than 16 and decreases gradually when N_{proj} is more than 360 and the mean error of W displacement is relatively small when $N_{proj} = 4$. That is may because all experiments used linear interpolation for FDK reconstruction. When the number of projection images is extremely small ($N_{proj} = 4$), the information obtained by linear interpolation occupies the most part and the simple deformation in these limited projections can be well reflected in the reconstructed volume image. when N_{proj} increase from 4 to 16, the projection data is still inadequate and the interpolation error caused by the increasing projections with noise may lead to a misdescription of deformation, thus an increase of mean error. With the further increase of N_{proj}, the volume image reconstructed by gradually sufficient projections can describe the deformation more accurately.

It can also be found that the decline rates of standard deviation error under different numbers of projections are not the same. In rescan experiment, the standard deviation errors of both displacement and strain decrease rapidly when N_{proj} increases from 4 to 36, while decrease gentle when N_{proj} exceeds 60. There still are some differences between rescan and compression experiments. The standard deviation error of displacement decreases faster with the increase of N_{proj} in the compression experiment and there is a sharp decline when N_{proj} increases from 360 to 720. Besides, unlike that the standard deviation of ϵ_{zz} with the sub-volume size of 21 × 21 × 21 voxels decreasing slowly when N_{proj} increases from 180 to 360 in the rescan experiment, there is an obvious rise in compression experiment. But overall, the trend of standard deviation error in these two real experiments is still analogous.

4.3. Discussion

From the results of the simulation experiment and the real experiment, it can be concluded that the mean errors and the standard deviation errors of displacement and strain show a downward trend with the increase of the number of projections. The mean errors, especially for strain, fluctuate when N_{proj} is small and then change little with the increase of N_{proj}. The standard deviation errors of the DVC measurement decrease rapidly at tens of N_{proj} but show a minor decrease when N_{proj} is larger than 200. Therefore, we can select the appropriate number of

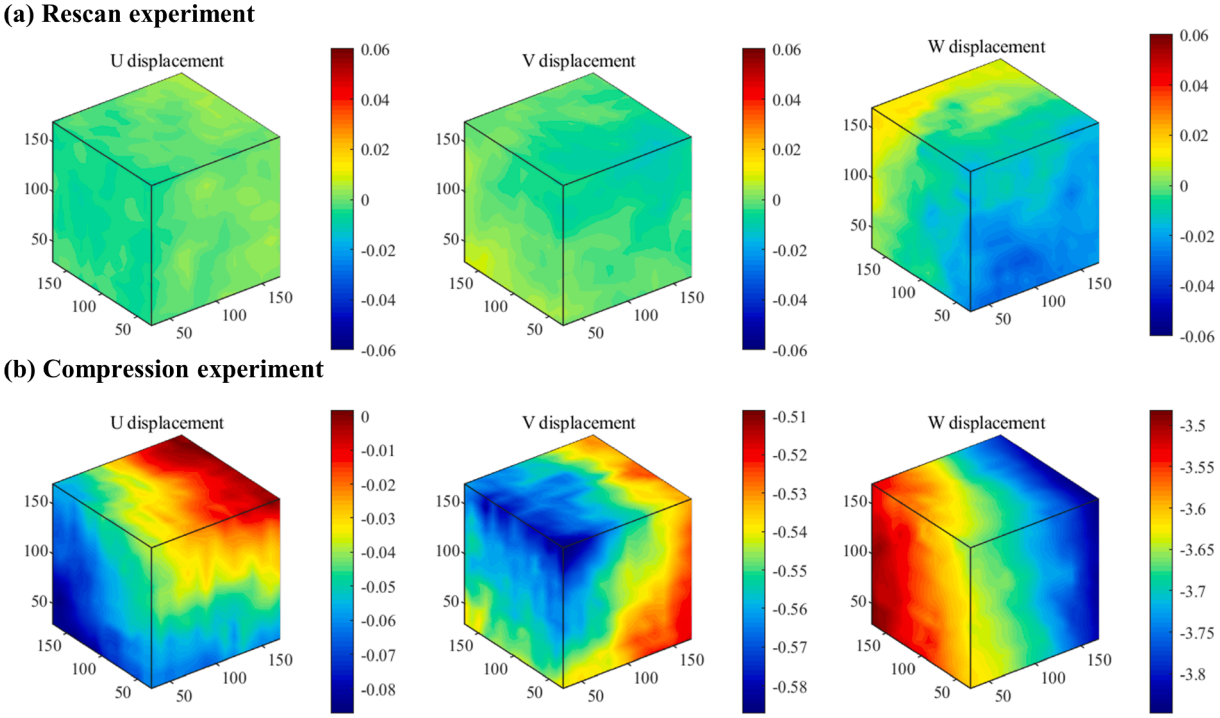

Fig. 10. The DVC displacement measurement with 1440 projections in foam copper (a) rescan and (b) compression experiments.

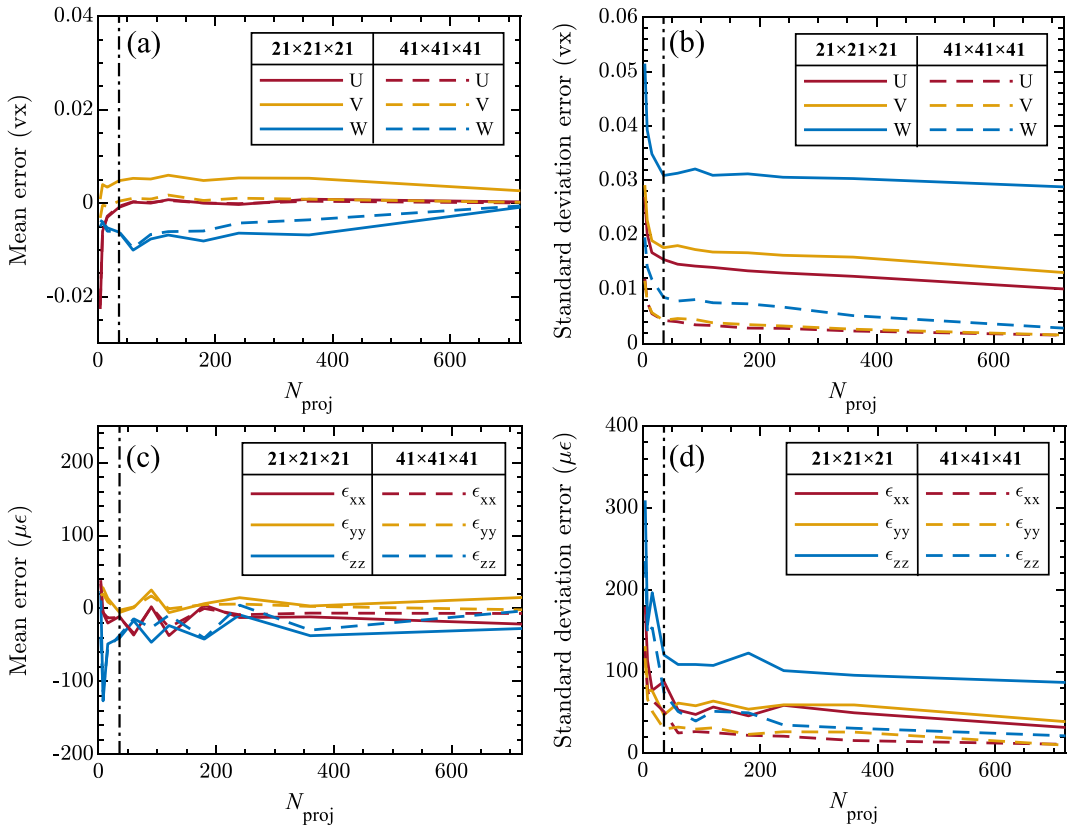

Fig. 11. Statistical results of DVC measurements on volume images reconstructed with different N_{proj} using two different sub-volume sizes in the foam copper resacn experiment: (a) mean error and (b) SD error in measured displacements, (c) mean error and (b) SD error in measured strains. Here the dash-dotted line is $N_{proj} = 36$, and vx denotes voxel.

projections based on these results according to the requirements of error levels (precision of DVC measurement) and imaging time (temporal resolution of DVC measurement). It is worth noting that only deformation along the rotation axis (except deformation caused by the Poisson effect) is considered in real compression experiment and there are differences in X-ray CT devices and micro-structures. Therefore, the number of projections recommended in this experiment may not be suitable for all cases.

To further evaluate the DVC calculation with different projection numbers, the average iteration times and the average ZNCC correlation coefficient are obtained and shown in Fig. 13. With the increase of N_{proj}, the DVC calculation generally has fewer times of iteration and a better correlation coefficient, which indicates that the efficiency and accuracy of DVC calculation are improved by degree. But in the real experiment, the average times of iterations with the sub-volume size of $21 \times 21 \times 21$ voxels increase greatly when N_{proj} rises from 360 to 720. This is mainly because the small size sub-volumes in the volume image reconstructed with adequate projections cannot contain rich intensity variations (as shown in Fig. 9), which may lead to a mismatch in DVC calculation. Increasing the sub-volume size from $21 \times 21 \times 21$ voxels to $41 \times 41 \times 41$ voxels can help to reduce the times of iteration but make little contribution to improve the correlation coefficient.

The mean intensity gradient (MIG) and image noise level (σ_n) can be used as speckle quality evaluation criteria of volume image in DVC calculation[29,30]. DVC measurements on volume images with larger MIG and lower noise levels have less error. The MIG and standard deviation of noises in volume images reconstructed with different projection numbers in the simulation experiment and real experiment were calculated. The Laplacian operator was used to estimate the standard deviation of volume image noise[31]. As shown in Fig. 14, both the noise standard deviation and MIG of reconstructed images decrease with the increase of N_{proj}. Therefore, increasing N_{proj} has a two-sided effect on the DVC measurement results. On the one hand, more projections could reduce the noise of reconstructed volume images and improve the accuracy of DVC measurement. On the other hand, larger N_{proj} would decrease the MIG of volume image, which would increase standard deviations during DVC measurement.

5. Conclusion

In this work, simulation and real experiments were carried out to study the effect of the number of projections of an X-ray CT device on the quality of reconstructed volume images and DVC measurements. Based on the experimental results, some valuable conclusions are summarized as follows:

1) The volume image reconstructed with more projections has higher fidelity thus better reconstruction quality. However, the volume image reconstructed with 240 projections is already of good quality despite that this number of projections does not satisfy the spatial Nyquist sampling theorem. Further increasing the number of projections shows little improvement on reconstructed volume image quality.
2) The DVC measurement errors, especially the standard deviation errors in detected displacements and strains, decrease with the increase of the number of projections at different decline rates. However, it is interesting to note that the DVC measurements on the volume images reconstructed with $36 \sim 60$ projections have similar error levels compared to those with more projections, even though these volume images have low fidelity and higher noise levels. This can be explained by the fact that the volume images reconstructed

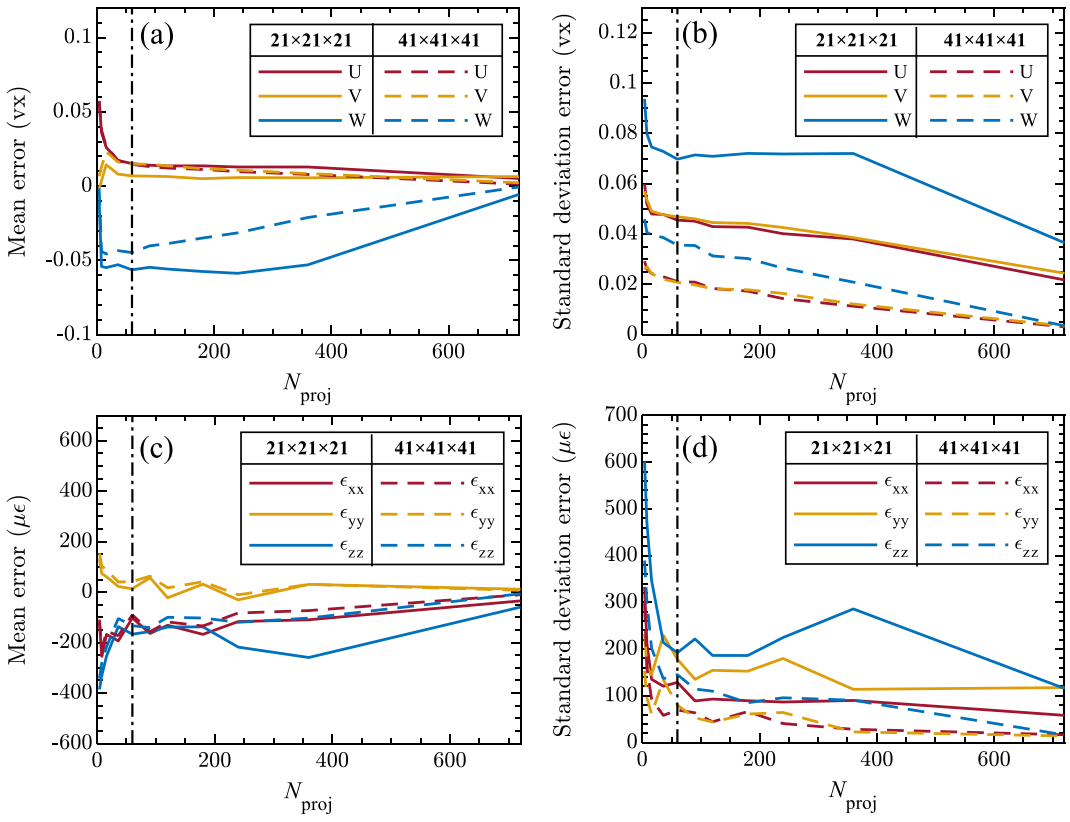

Fig. 12. Statistical results of DVC measurements on volume images reconstructed with different N_{proj} using two different sub-volume sizes in the foam copper compression experiment. (a) mean error and (b) SD error in measured displacements, (c) mean error and (b) SD error in measured strains. Here the dash-dotted line is $N_{\text{proj}} = 60$, and vx denotes voxel.

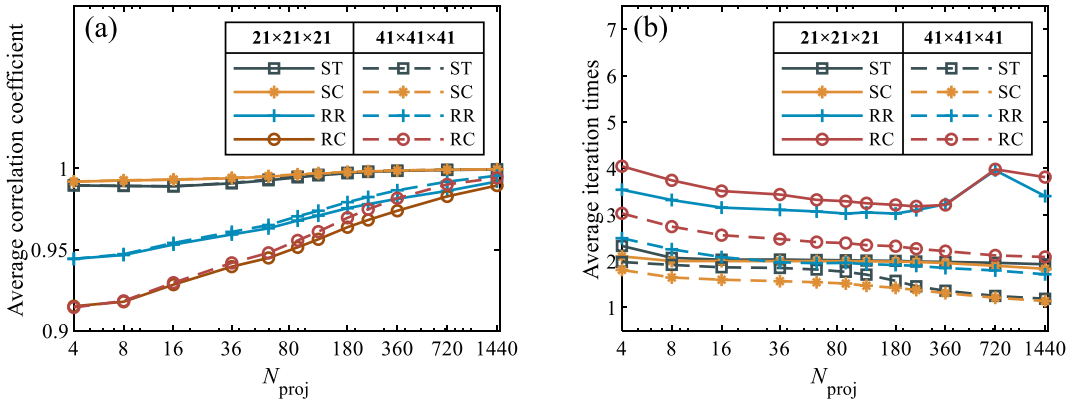

Fig. 13. (a)The average iteration times and (b) the average correlation coefficient of DVC calculations with two sub-volume sizes in simulation experiment (ST: simulated translation, SC: simulated compression) and real experiment (RR: real rescan, RC: real compression).

with few projections have higher MIG values, which can still use as a faithful deformation carrier.

3) Appropriate number of projections can be selected according to actual requirements of measurement precision and temporal resolution. Given the copper foam sample and X-ray CT equipment in this real experiment, it is recommended to reconstruct the volume image with 36 ~ 60 projections, which can obtain relatively accurate results (acceptable measurement precision) with less sampling time (high temporal resolution). If the temporal resolution is not considered, more than reconstruction with 720 projections is better to ensure more precise DVC measurements.

There are two recently developed methods for improving the temporal resolution: 1) projection-based DVC[32] is an integrated method (back-projection reconstruction and deformation measurement), whose measurement quality still depends on the selection of the number of projections. 2) High-speed acquisition[33] relies on an improvement of hardware equipment (e.g., synchrotron radiation). However, the fundamental problem is that the increased temporal resolution will inevitably weaken the quality of DVC measurements. Therefore, this work aims at investigating the effect of the number of projections on DVC measurements with X-ray CT and providing certain referential suggections for balancing measurement accuracy and temporal resolutions during practical DVC applications through regulating projection numbers. However, different numbers of projections were acquired in simulation and real experiments by evenly extracting the

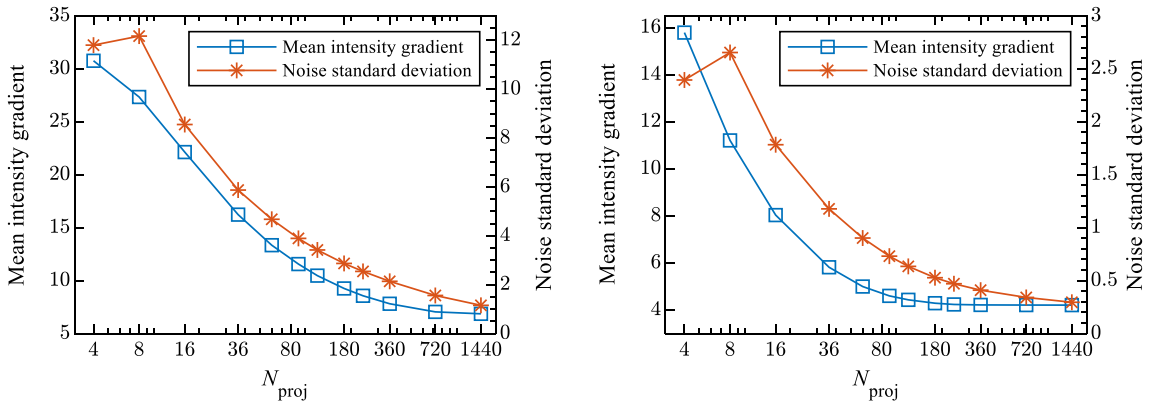

Fig. 14. The mean intensity gradient and standard deviation of noises in volume images reconstructed with different N_{proj} in simulation experiment(left) and real experiment(right).

maximum number of projection images, which are a little different from projections acquired in practice. Besides, the suggestions given in this work might vary with different deformation situations, micro-structures, and X-ray CT devices in practice. And whether the conclusions can be extended to other X-ray CT devices or deformation cases, more experimental works should be performed.

CRediT authorship contribution statement

Zhang Xuanhao: Methodology, Investigation, Formal analysis, Data curation, Writing – original draft, Visualization. **Sun Lijuan:** Validation. **Wang Bo:** Software, Writing – review & editing. **Pan Bing:** Conceptualization, Project administration, Funding acquisition.

Declaration of Competing Interest

The authors declare that they have no known competing financial interests or personal relationships that could have appeared to influence the work reported in this paper.

Acknowledgements

This work was supported by National Natural Science Foundation of China (Grant nos. 11925202, 11872009).

References

[1] B.K. Bay, T.S. Smith, D.P. Fyhrie, M. Saad, Digital volume correlation: Three-dimensional strain mapping using X-ray tomography, Exp. Mech. 39 (1999) 217–226.
[2] J.Y. Buffiere, E. Maire, J. Adrien, J.P. Masse, E. Boller, In situ experiments with X ray tomography: an attractive tool for experimental mechanics, Exp. Mech. 50 (2010) 289–305.
[3] N. Limodin, J. Réthoré, J. Adrien, J.Y. Buffière, F. Hild, S. Roux, Analysis and artifact correction for volume correlation measurements using tomographic images from a laboratory X-ray source, Exp. Mech. 51 (2010) 959–970.
[4] L. Mao, Z. Yuan, M. Yang, H. Liu, F.-P. Chiang, 3D strain evolution in concrete using in situ X-ray computed tomography testing and digital volumetric speckle photography, Measurement 133 (2019) 456–467.
[5] A. Benoit, S. Guérard, B. Gillet, G. Guillot, F. Hild, D. Mitton, J. Périé, S. Roux, 3D analysis from micro-MRI during in situ compression on cancellous bone, J. Biomech. 42 (2009) 2381–2386.
[6] J. Fu, F. Pierron, P.D. Ruiz, Elastic stiffness characterization using three-dimensional full-field deformation obtained with optical coherence tomography and digital volume correlation, J. Biomed. Opt. 18 (2013) 121512.
[7] E.M. Dan, H.A. Quigley, T.D. Nguyen, In vivo characterization of the deformation of the human optic nerve head using optical coherence tomography and digital volume correlation, Acta Biomater. 96 (2019) 385–399.
[8] C. Franck, S. Hong, S.A. Maskarinec, D.A. Tirrell, G. Ravichandran, Three-dimensional full-field measurements of large deformations in soft materials using confocal microscopy and digital volume correlation, Exp. Mech. 47 (2007) 427–438.
[9] L.A. Feldkamp, L.C. Davis, J.W. Kress, Practical cone-beam algorithm, J. Opt. Soc. Am. A 1 (6) (1984) 612.
[10] A. Du Plessis, C. Broeckhoven, A. Guelpa, S.G. Le Roux, Laboratory X-ray micro-computed tomography: a user guideline for biological samples, GigaScience 6 (2017) 1–11.
[11] A. Manmadhachary, Y. Ravi Kumar, L. Krishnanand, Effect of CT acquisition parameters of spiral CT on image quality and radiation dose, Measurement 103 (2017) 18–26.
[12] E.A. Zwanenburg, M.A. Williams, J.M. Warnett, Review of high-speed imaging with lab-based x-ray computed tomography, Meas. Sci. Technol. 33 (2021) 012003.
[13] Z. Zhao, G.J. Gang, J.H. Siewerdsen, Noise, sampling, and the number of projections in cone-beam CT with a flat-panel detector, Med. Phys. 41 (2014) 061909.
[14] H. Villarraga-Gómez, S.T. Smith, Effect of the number of projections on dimensional measurements with X-ray computed tomography, Precis. Eng. 66 (2020) 445–456.
[15] B.P. Croom, D. Burden, H. Jin, N.H. Vonk, J.P.M. Hoefnagels, B. Smaniotto, F. Hild, E. Quintana, Q. Sun, X. Nie, X. Li, Interlaboratory study of digital volume correlation error due to X-ray computed tomography equipment and scan parameters: an update from the DVC challenge, Exp. Mech. 61 (2020) 395–410.
[16] Y. Wang, P. Lava, P. Reu, D. Debruyne, Theoretical analysis on the measurement errors of local 2D DIC: part I temporal and spatial uncertainty quantification of displacement measurements, Strain 52 (2016) 110–128.
[17] A.C. Kak, M. Slaney, G. Wang, Principles of Computerized Tomographic Imaging, Medical Physics, 29 (2002) 107-107.
[18] Z. Fang, H. Gong, G. Yang, T. Zhang, Effect of projection number on slice image quality of micro-CT system, SPIE, 2009.
[19] A. Buljac, C. Jailin, A. Mendoza, J. Neggers, T. Taillandier-Thomas, A. Bouterf, B. Smaniotto, F. Hild, S. Roux, Digital volume correlation: review of progress and challenges, Exp. Mech. 58 (2018) 1–48.
[20] B. Wang, B. Pan, R. Tao, G. Lubineau, Systematic errors in digital volume correlation due to the self-heating effect of a laboratory X-ray CT scanner, Meas. Sci. Technol. 28 (5) (2017) 055402.
[21] L. Turpin, S. Roux, O. Caty, S. Denneulin, S. Brunetti, P. Dulio, A. Frosini, G. Rozenberg, A phase field approach to limited-angle tomographic reconstruction, Fundamenta Informaticae 172 (2) (2020) 203–219.
[22] G.N. Ramachandran, A.V. Lakshminarayanan, Three-dimensional reconstruction from radiographs and electron micrographs: application of convolutions instead of fourier transforms, Proc Natl Acad Sci U S A 68 (9) (1971) 2236–2240.
[23] B. Pan, B. Wang, D. Wu, G. Lubineau, An efficient and accurate 3D displacements tracking strategy for digital volume correlation, Opt. Lasers Eng. 58 (2014) 126–135.
[24] B. Pan, D. Wu, Z. Wang, Internal displacement and strain measurement using digital volume correlation: a least-squares framework, Meas. Sci. Technol. 23 (2012).
[25] B. Pan, H. Xie, Z. Wang, Equivalence of digital image correlation criteria for pattern matching, Appl. Opt. 49 (2010) 5501–5509.
[26] B. Pan, B. Wang, A flexible and accurate digital volume correlation method applicable to high-resolution volumetric images, Meas. Sci. Technol. 28 (2017) 105007-.
[27] B. Münch, P. Trtik, F. Marone, M. Stampanoni, Stripe and ring artifact removal with combined wavelet–Fourier filtering, Opt. Express 17 (2009) 8567–8591.
[28] A. Biguri, M. Dosanjh, S. Hancock, M. Soleimani, TIGRE: a MATLAB-GPU toolbox for CBCT image reconstruction, Biomedical Physics & Engineering Express, 2 (2016) 055010.
[29] Y.Q. Wang, M.A. Sutton, H.A. Bruck, H.W. Schreier, Quantitative error assessment in pattern matching: effects of intensity pattern noise, interpolation, strain and image contrast on motion measurements, Strain 45 (2009) 160–178.
[30] B. Pan, Z. Lu, H. Xie, Mean intensity gradient: an effective global parameter for quality assessment of the speckle patterns used in digital image correlation, Opt. Lasers Eng. 48 (2010) 469–477.

[31] S.C. Tai, S.M. Yang, A fast method for image noise estimation using Laplacian operator and adaptive edge detection, International Symposium on, Communications (2008).

[32] C. Jailin, S. Roux, D. Sarrut, S. Rit, Projection-based dynamic tomography, Phys. Med. Biol. 66 (2021) 215018.

[33] E. Maire, C. Le Bourlot, J. Adrien, A. Mortensen, R. Mokso, 20 Hz X-ray tomography during an in situ tensile test, Int. J. Fract. 200 (1-2) (2016) 3–12.